Linker-based Bandgap Tuning in Conductive MOF Solid Solutions

Ji Yong Choi,[a] Minyan Wang,[b] Brianna Check,[a] Michael Stodolka,[a] Kyle Tayman,[a] Sandeep Sharma,*[a] and Jihye Park*[a]

[a] Dr. J. Y. Choi, B. Check, M. Stodolka, K. Tayman, Prof. S. Sharma, and Prof. J. Park
Department of Chemistry
University of Colorado Boulder
Boulder, Colorado 80309, United States
E-mail: Jihye.Park@colorado.edu

[b] M. Wang
Materials Science & Engineering Program
University of Colorado Boulder
Boulder, Colorado 80303, United States

Supporting information for this article is given via a link at the end of the document.

Abstract: Herein, we report the synthesis of $Cu_3(HAB)_x(TATHB)_{2-x}$ (HAB: hexaaminobenzene, TATHB: triaminotrihydroxybenzene). Synthetic improvement of pure-phase $Cu_3(TATHB)_2$ led to a more crystalline framework with higher electrical conductivity value than the previously reported. The improved crystallinity and analogous structure between TATHB and HAB enabled us to synthesize $Cu_3(HAB)_x(TATHB)_{2-x}$ with ligand compositions precisely controlled by precursor ratios. The electrical conductivity was tuned from 4.2×10^{-8} S cm^{-1} to 2.9×10^{-5} S cm^{-1} by simply increasing the nitrogen content in the crystal lattice. Furthermore, computational calculation supports that the solid solution facilitates the band structure tuning. We envision that our findings not only shed light on the ligand-dependent structure-property relationship but create new prospects in synthesizing multicomponent electrically conductive MOFs for tailoring optoelectronic device applications.

Introduction

Fine-tuning of electronic band structure is one of the key design strategies in material science for various applications, including optoelectronics, solar cells, batteries, photocatalysis, and electrocatalysis.[1–8] For example, photovoltaic applications require bandgap engineering to improve light absorption and maximize the power conversion efficiency.[9] In addition, transistors need precise band alignment to optimize charge injection efficiency at the heterojunction interfaces.[10] To realize the fine tunability at the practical level, solid solutions, a homogeneous mixture of solids in a single-phase crystalline platform are widely used through varying the composition of materials.[11,12]

In this work, we adopted the solid solution concept to electrically conductive metal-organic frameworks (MOFs), a rapidly emerging class of porous (semi)conductors.[13] The impact of engineering their electronic structure is powerful to their performance for electrocatalysis and chemiresistive sensors.[14–17] However, tuning the electronic properties of conductive MOFs are conditional due to the limited number of choices in metal nodes and linkers. Instead, MOF solid solutions can be a promising approach by exhibiting continuous tunability in principle utilizing the existed metal nodes and linkers.

For instance, Dincă and coworkers reported binary metal-alloyed conjugated MOFs, $(M_xM'_{3-x})(HITP)_2$ (MM' = CuNi, CoNi, CoCu; HITP = 2,3,6,7,10,11-hexaiminotriphenylene), and demonstrated that both bandgap and electrical conductivity were tunable by adjusting binary metal ratios.[18] Kitagawa and coworkers reported an interesting mixed-ligand conductive MOF, Cu_3(HHTP)(THQ) (HHTP: 2,3,6,7,10,11-

This is the author manuscript accepted for publication and has undergone full peer review but has not been through the copyediting, typesetting, pagination and proofreading process, which may lead to differences between this version and the Version of Record. Please cite this article as doi: 10.1002/smll.202206988.

hexahydroxytriphenylene, THQ: tetrahydroxy-1,4-quinone) where the two composing ligands have different sizes, thus creating new crystal lattices.[19] Yet, these systems still left a room for further exploration for fine-tuning of their electronic properties.

Ligand-based solid solutions are rare, likely due to their bulky size and different reactivity from their respective functional groups, making it difficult to form a single-phase crystal structure.[20,21] For example, hexaaminobenzene (HAB) and hexahydroxybenzene (HHB) are similarly sized with the only difference in coordinating atoms but the synthetic conditions for making their isostructural MOFs are markedly different.[22,23]

Herein, we present the synthesis of two-dimensional $Cu_3(TATHB)_2$ (TATHB: triaminotrihydroxybenzene), namely Cu-TATHB. Although Cu-TATHB has been reported,[24] we have developed a new synthetic procedure for a high-quality crystalline structure, which enabled successful synthesis of an isostructural solid solution system, $Cu_3(HAB)_x(TATHB)_{2-x}$. We demonstrate a precise control of electronic properties with varied HAB/TATHB ratios in the crystal lattice. The resulting solid solutions exhibited a continuous shift in band energies and an increase of conductivity over 3 orders of magnitude as the nitrogen content increases with higher HAB ratio to TATHB in the crystal lattice. Furthermore, density functional theory (DFT) calculations corroborate our experimental results in that band alignment can be continuously tuned as nitrogen density increases in the solid solution system.

Results and Discussion

Synthesis and Characterizations

We chose Cu-TATHB as a starting MOF for $Cu_3(HAB)_x(TATHB)_{2-x}$. We hypothesized that amine groups in TATHB can give synthetic similarity with HAB, while hydroxyl groups can impose different electronic properties in the MOF solid solutions. Additionally, we expected that TATHB enables fine control of nitrogen content in the crystal lattice of solid solutions compared to using HHB.

Cu-TATHB was hydrothermally synthesized, where TATHB ligands reacted with $Cu(NO_3)_2{\cdot}2.5H_2O$ in water (Figure 1a). We investigated a series of synthetic parameters, including concentration, base addition sequence, and reaction time (Figure S1-S3. See the SI for details of synthesis optimization). Compared to previously reported Cu-TATHB, we observed that using ammonium hydroxide as a base and optimizing the reaction time substantially improve the crystallinity by adjusting the rate of ligand's deprotonation, nucleation, and crystal growth. The resulting structure of Cu-TATHB was refined against Pawley fit based on synchrotron powder X-ray diffraction (PXRD) (λ = 0.45237 Å) (Figure 1b). The afforded Cu-TATHB shows a good agreement with an AA eclipsed stacking (Figure S4). Cu-TATHB shows a hexagonal unit cell with the space group of *P6/m* having cell parameters of $a = b = 13.2786$ and $c = 3.3228$ (residue $R_{wp} = 1.29\%$, Table S1). The distinct diffraction at $2\theta = 2.20°$ represents a hexagonal pore with $d_{100} = 11.78$ Å and the peak at 8.08° corresponds to the interlayer spacing of 3.21 Å. Our results slightly differ from the previously reported Cu-TATHB, which adopted the slipped-parallel packing.[24]

Fourier transform infrared (FTIR) spectroscopy shows the peaks around 1230 cm^{-1} and 1032 cm^{-1}, assigned to C-N and C-O stretching bands, respectively (Figure 1c). The peaks shifted to lower wavenumbers than those for the TATHB ligand, suggesting the formation of a delocalized MOF by coordinating copper nodes with TATHB.[25] Next, the surface area was measured by N_2 sorption isotherm at 77 K. Compared to the previously reported Brunauer-Emmett-Teller (BET) surface area of Cu-TATHB (33 $m^2\ g^{-1}$),[24] our MOF product shows a much improved surface area of 160 $m^2\ g^{-1}$ (Figure 1d). The higher surface area would be due to the improved crystallinity and the eclipsed packing mode. Scanning electron microscopy (SEM) and transmission electron microscopy (TEM) images show rod morphology in ~50 nm length (Figure 1e and Figure S5). High-resolution TEM (HRTEM) images revealed a clearly ordered structure with a channel width of 11.60 Å, which corroborates PXRD analysis.

The survey scan of X-ray photoelectron spectroscopy (XPS) revealed that the atomic ratio of N:O in Cu-TATHB is 1:1.08 and (O+N):Cu is 4.09:1, corroborating a chemical formula is $Cu_3(TATHB)_2$ (Figure S6a, Table S2). A high-resolution Cu $2p_{3/2}$ spectrum exhibits two major deconvoluted peaks: the binding energy at 933 eV and 935.2 eV that are attributed to Cu(0/I) and Cu(II), respectively (Figure S6b).[26] The O 1s spectra exhibit both C-O and C=O signals (Figure S6c), and the N 1s spectra reveal both a quinoid imine (=N-) and a benzoid amine (-NH-) (Figure S6d),[22,27] corroborating that two different coordinating groups in TATHB are coordinated to the metal node.

Electronic Properties Characterizations

Encouraged by structural characterizations, the electronic structure of Cu-TATHB was investigated by UV-vis-NIR spectroscopy. Cu-TATHB exhibits a strong absorption at 630 nm extending to the near-infrared region due to strong d-π conjugation (Figure 2a). Tauc plot derived from the absorption spectrum determined the optical bandgap to be 0.98 eV. Then, we measured the electrical conductivity on a pressed pellet via the four-point probe method. Under ambient conditions, Cu-TATHB exhibited

an electrical conductivity of 4.2 × 10^{-8} S cm^{-1}. Although insulating,[24] high crystallinity might allow a long-range delocalization, which aided charge transport throughout the framework. Temperature-dependent conductivity was studied in the temperature range from 293 K to 343 K under vacuum (Figure 2b). By fitting to the Arrhenius equation, $\sigma = \sigma_0 \exp(-E_a/k_BT)$, where σ_0 is a prefactor, E_a is the thermal activation energy, k_B is Boltzmann constant, and T is the absolute temperature, E_a was calculated to be 0.33 eV, implying Cu-TATHB behaves like a typical semiconducting material.

Ligand-based MOF Solid Solutions

We propose a binary solid solution of $Cu_3(HAB)_x(TATHB)_{2-x}$ by changing the feed ratios of TATHB to HAB between 3:1, 1:1, and 1:3 (Figure 3a), which will change the theoretical nitrogen content from 50% to 62.5%, 75%, 87.5%, and 100%. Comparing N/O atomic ratios in SEM energy dispersive X-ray spectroscopy (EDS) confirmed that the HAB/TATHB ratios in the MOFs are proportional to the feed ratio of corresponding precursors (Table S3). Additionally, we carried out ^{1}H NMR analysis to quantitatively probe the relative molar ratios of the TATHB and HAB by decomposing 5 mg of samples with DCl in D_2O. ^{1}H NMR analysis reveals that the HAB to TATHB ratios are 1:2.6, 1:0.9, and 2.7:1, which match well to the theoretical values (Table S4).

As shown in Figure 3b, synchrotron PXRD confirmed all series of MOF solid solutions represent the same hexagonal structure. Whereas, UV-vis-NIR absorption spectroscopy gave insight into the variations in electronic structures with respect to HAB/TATHB ratio (Figure S7). The Tauc plots derived from each absorption spectrum indicate that the optical bandgap shifts from 0.98 eV to 0.96 eV, 0.94 eV, 0.92 eV, and 0.91 eV as the HAB content increases (Figure 3c and Figure S8).

The morphology of $Cu_3(HAB)_x(TATHB)_{2-x}$ samples show gradual change in aspect ratio as the HAB content increases (Figure 3d,e and Figure S5). As the amount of HAB increased, the average particle size on the long side decreased from approximately 50 nm to 27 nm, while the short side increased from 11 nm to 18 nm (Figure 3d). SEM-EDS elemental mapping of $Cu_3(HAB)_x(TATHB)_{2-x}$ samples revealed a uniform distribution of O and N atoms, supporting the formation of solid solution rather than inhomogeneous segregation of Cu-TATHB and Cu-HAB. Additionally, we attempted synthesis of solid solutions, combination of THQ with HAB or TATHB as a control experiment. THQ is a partial oxidation product of HHB, which is proven to form Cu-THQ, exhibiting an identical structure to Cu-HHB.[23] However, the results revealed that THQ was incompatible for synthesizing the previously reported Cu-TATHB was reported to be solid solution with the other isostructural ligands, perhaps due to different oxidation state and the favored stacking mode being different when forming MOFs (slipped parallel for Cu-THQ vs. eclipsed for Cu-TATHB and Cu-HAB) (Figure S9).

DFT Calculation

To further understand the intrinsic electronic structure of $Cu_3(HAB)_x(TATHB)_{2-x}$, DFT calculations were performed based on $Cu_3(TATHB)_2$, $Cu_3(HAB)(TATHB)$, and $Cu_3(HAB)_2$. The path of high symmetry **k**-points of hexagonal MOFs in the first Brillouin zone is depicted as Figure 4a. The bands of all three samples cross the Fermi level in the out-of-plane direction (Γ–A, L–M, and H-K), which indicate a metallic character (Figure S10). However, metallic properties were excluded from our system because charge transport within the d-π conjugated planes is considered to be the dominant pathway for electrical conductivity in the 2D system.[13,28]

On the other hand, projected densities of states (PDOS) calculations along the in-plane directions (Γ–M, M–K, and K–Γ) reveal that the valence band and conduction band are composed of the p_z orbitals of C, N, O and d_{x2-y2} orbital of Cu, indicating that the typical d-π conjugation governs the electronic structure. Moreover, the in-plane band structures show that $Cu_3(HAB)_2$ is metallic, while no bands cross the Fermi level for $Cu_3(HAB)(TATHB)$ and $Cu_3(TATHB)_2$ with a calculated bandgap of 0.35 eV and 0.70 eV, respectively (Figure 4b-d). These results show a strong correlation with the bandgap decreases as the HAB concentration increases, corroborating the experimental optical bandgap measured.

Tuning of Electronic Properties

We measured the lowest unoccupied molecular orbital (LUMO) energy levels via cyclic voltammetry (CV).[29] The MOF particles were drop-casted on a glassy carbon electrode as the working electrode and Ag/Ag^+ was used as the reference electrode. The onset reduction potential was read for calculating the LUMO level with reference to the Fc/Fc^+ (Fc: ferrocene) redox couple (See the Experimental Section for the details). As shown in Figure 5a and S11, the onset potential shifted from -1.09 V to -1.16 V as the HAB ratio increases. The highest occupied molecular orbital (HOMO) levels were then calculated using the optical bandgaps to complete the band alignments of the materials. A gradual shift of HOMO level is due to variation in HAB/TATHB ratio considering orbital overlap between HOMO of linker would be most responsible for the bands of the resulting MOFs with the fixed metal node species (Figure 5b).

Lastly, a bulk electrical conductivity of $Cu_3(HAB)_x(TATHB)_{2-x}$ revealed that the values can be precisely tuned over 3 orders of magnitude from 4.2×10^{-8} S cm^{-1} to 2.9×10^{-5} S cm^{-1} as the HAB ratio increases (Figure 5c). In addition, the corresponding activation energies varied linearly, suggesting continuous band engineering through mixed linkers in the lattice (Figure 5d). We measured the electrical conductivity of the physical mixtures between $Cu_3(TATHB)_2$ and $Cu_3(HAB)_2$ as a control experiment. As expected, the mechanically blended mixtures show no clear trend in conductivity changes with respect to HAB/TATHB ratios (Figure S12).

Conclusion

Solid solutions allow fine compositional tuning of nitrogen density in the lattice of $Cu_3(HAB)_x(TATHB)_{2-x}$, which tailored the band alignment and improved an electrical conductivity over 3 orders of magnitude. Computational calculations further supported that the different atomic composition in the reference crystal lattice indeed facilitates the band structure tuning. Our results showcase the fine tuning of the electronic structure of conductive MOFs, which will be crucial for optimizing the performance of electronic materials.

Acknowledgements

J.P. acknowledges the start-up funds from the University of Colorado Boulder. J.Y.C. acknowledges support by the Postdoctoral Fellowship from the National Research Foundation of Korea under grant no. NRF-2021R1A6A3A14044659. M.W and S.S. were supported through the NSF grant CHE-2145209. Use of the Advanced Photon Source was supported by the U.S. Department of Energy, Office of Science, Office of Basic Energy Sciences, under Contract No. DE-AC02-06CH11357. We thank Kori Smyser for doing the DFT optimizations.

Keywords: metal-organic framework • electrical conductivity • solid solution • bandgap tuning

[1] H. Arandiyan, S. S. Mofarah, C. C. Sorrell, E. Doustkhah, B. Sajjadi, D. Hao, Y. Wang, H. Sun, B.-J. Ni, M. Rezaei, Z. Shao, T. Maschmeyer, *Chem. Soc. Rev.* **2021**, *50*, 10116–10211.

[2] Z. Xia, S. Guo, *Chem. Soc. Rev.* **2019**, *48*, 3265–3278.

[3] W. Yang, B. Liu, B. Yang, J. Wang, T. Sekiguchi, S. Thorsten, X. Jiang, *Adv. Funct. Mater.* **2015**, *25*, 2543–2551.

[4] Y. Zhen, H. Tanaka, K. Harano, S. Okada, Y. Matsuo, E. Nakamura, *J. Am. Chem. Soc.* **2015**, *137*, 2247–2252.

[5] L. Zhou, A. Assoud, Q. Zhang, X. Wu, L. F. Nazar, *J. Am. Chem. Soc.* **2019**, *141*, 19002–19013.

[6] S. Jin, Y. Ye, Y. Niu, Y. Xu, H. Jin, J. Wang, Z. Sun, A. Cao, X. Wu, Y. Luo, H. Ji, L.-J. Wan, *J. Am. Chem. Soc.* **2020**, *142*, 8818–8826.

[7] C. Zhang, C. Xie, Y. Gao, X. Tao, C. Ding, F. Fan, H.-L. Jiang, *Angew. Chem. Int. Ed.* **2022**, *61*, e202204108.

[8] H. Lin, Y. Xu, B. Wang, D.-S. Li, T. Zhou, J. Zhang, *Small Struct.* **2022**, *3*, 2100176.

[9] A. Polman, M. Knight, E. C. Garnett, B. Ehrler, W. C. Sinke, *Science* **2016**, *352*, aad4424–aad4424.

[10] R. Begum, M. R. Parida, A. L. Abdelhady, B. Murali, N. M. Alyami, G. H. Ahmed, M. N. Hedhili, O. M. Bakr, O. F. Mohammed, *J. Am. Chem. Soc.* **2017**, *139*, 731–737.

[11] F. Hao, C. C. Stoumpos, R. P. H. Chang, M. G. Kanatzidis, *J. Am. Chem. Soc.* **2014**, *136*, 8094–8099.

[12] J. Zhao, S. M. Islam, O. Y. Kontsevoi, G. Tan, C. C. Stoumpos, H. Chen, R. K. Li, M. G. Kanatzidis, *J. Am. Chem. Soc.* **2017**, *139*, 6978–6987.

[13] L. S. Xie, G. Skorupskii, M. Dincă, *Chem. Rev.* **2020**, *120*, 8536–8580.

[14] A. J. Clough, J. W. Yoo, M. H. Mecklenburg, S. C. Marinescu, *J. Am. Chem. Soc.* **2015**, *137*, 118–121.

[15] C. A. Downes, A. J. Clough, K. Chen, J. W. Yoo, S. C. Marinescu, *ACS Appl. Mater. Interfaces* **2018**, *10*, 1719–1727.

[16] Z. Meng, A. Aykanat, K. A. Mirica, *J. Am. Chem. Soc.* **2019**, *141*, 2046–2053.

[17] V. Rubio-Giménez, N. Almora-Barrios, G. Escorcia-Ariza, M. Galbiati, M. Sessolo, S. Tatay, C. Martí-Gastaldo, *Angew. Chem. Int. Ed.* **2018**, *57*, 15086–15090.

[18] T. Chen, J.-H. Dou, L. Yang, C. Sun, N. J. Libretto, G. Skorupskii, J. T. Miller, M. Dincă, *J. Am. Chem. Soc.* **2020**, *142*, 12367–12373.

[19] M.-S. Yao, J.-J. Zheng, A.-Q. Wu, G. Xu, S. S. Nagarkar, G. Zhang, M. Tsujimoto, S. Sakaki, S. Horike, K. Otake, S. Kitagawa, *Angew. Chem. Int. Ed.* **2020**, *59*, 172–176.

[20] A. D. Burrows, *CrystEngComm* **2011**, *13*, 3623–3642.

[21] C. Schlüsener, M. Xhinovci, S.-J. Ernst, A. Schmitz, N. Tannert, C. Janiak, *Chem. Mater.* **2019**, *31*, 4051–4062.

[22] J. Park, M. Lee, D. Feng, Z. Huang, A. C. Hinckley, A. Yakovenko, X. Zou, Y. Cui, Z. Bao, *J. Am. Chem. Soc.* **2018**, *140*, 10315–10323.

[23] J. Park, A. C. Hinckley, Z. Huang, D. Feng, A. A. Yakovenko, M. Lee, S. Chen, X. Zou, Z. Bao, *J. Am. Chem. Soc.* **2018**, *140*, 14533–14537.

[24] Y. Jiang, I. Oh, S. H. Joo, Y.-S. Seo, S. H. Lee, W. K. Seong, Y. J. Kim, J. Hwang, S. K. Kwak, J.-W. Yoo, R. S. Ruoff, *J. Am. Chem. Soc.* **2020**, *142*, 18346–18354.

[25] K. I. Hadjiivanov, D. A. Panayotov, M. Y. Mihaylov, E. Z. Ivanova, K. K. Chakarova, S. M. Andonova, N. L. Drenchev, *Chem. Rev.* **2021**, *121*, 1286–1424.

[26] J. Y. Choi, J. Park, *ACS Appl. Electron. Mater.* **2021**, *3*, 4197–4202.

[27] M. Smith, L. Scudiero, J. Espinal, J.-S. McEwen, M. Garcia-Perez, *Carbon* **2016**, *110*, 155–171.

[28] J.-H. Dou, L. Sun, Y. Ge, W. Li, C. H. Hendon, J. Li, S. Gul, J. Yano, E. A. Stach, M. Dincă, *J. Am. Chem. Soc.* **2017**, *139*, 13608–13611.

[29] J. Mahmood, E. K. Lee, M. Jung, D. Shin, I.-Y. Jeon, S.-M. Jung, H.-J. Choi, J.-M. Seo, S.-Y. Bae, S.-D. Sohn, N. Park, J. H. Oh, H.-J. Shin, J.-B. Baek, *Nat. Commun.* **2015**, *6*, 6486.

Entry for the Table of Contents

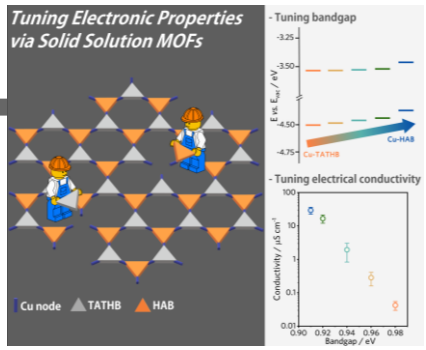

We report the synthesis of electrically conductive MOF solid solutions $Cu_3(HAB)_x(TATHB)_{2-x}$ (HAB: hexaaminobenzene, TATHB: triaminotrihydroxybenzene), exhibiting an increase of conductivity over 3 orders of magnitude and capable of tailoring band alignment as the HAB content increases.

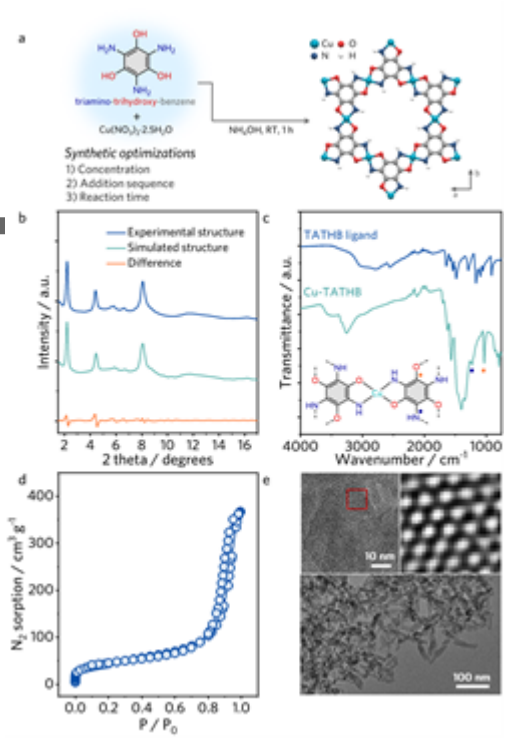

Figure 1. (a) Synthetic scheme of Cu-TATHB. (b) Experimental synchrotron PXRD data of Cu-TATHB collected at beamline 17-BM at the Advanced Photon Source, Argonne National Laboratory, USA (λ = 0.45237 Å). (c) FTIR spectra, (d) N_2 sorption isotherm, and (e) TEM image of Cu-TATHB. The insets in (e) represent HRTEM image and simulated pore structure after inverse fast Fourier transform based on the red box.

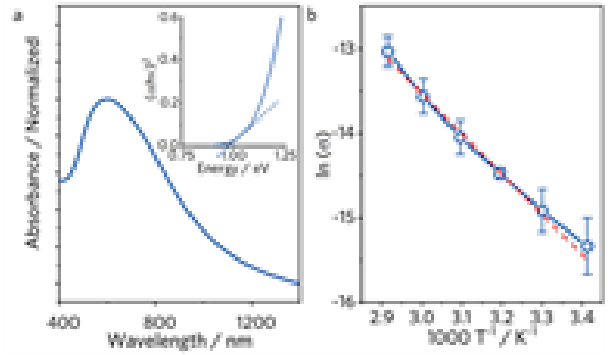

Figure 2. (a) UV-vis-NIR absorption spectroscopy and (b) Arrhenius fitting of temperature-dependent electrical conductivity under vacuum.

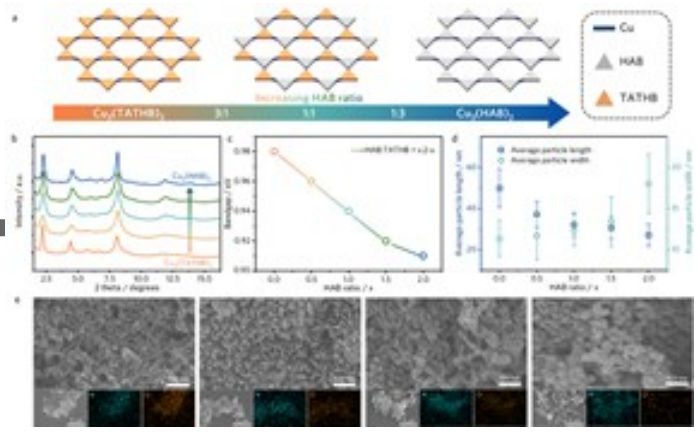

Figure 3. (a) Schematic representation, (b) synchrotron PXRD data, (c) optical bandgaps, and (d) variations on crystal length and width of $Cu_3(HAB)_x(TATHB)_{2-x}$ (x = 0, 0.5, 1, 1.5, and 2). (e) SEM images of $Cu_3(HAB)_{0.5}(TATHB)_{1.5}$, $Cu_3(HAB)(TATHB)$, $Cu_3(HAB)_{1.5}(TATHB)_{0.5}$, and $Cu_3(HAB)_2$ with SEM-EDS elemental mapping for N and O.

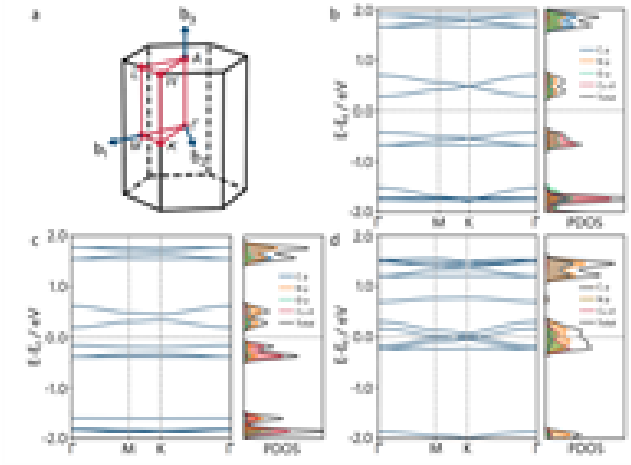

Figure 4. (a) The first Brillouin zone of a hexagonal cell with the high symmetry k-point path marked in red. In-plane band structure and projected density of states for the (b) $Cu_3(TATHB)_2$, (c) $Cu_3(HAB)(TATHB)$, and (d) $Cu_3(HAB)_2$.

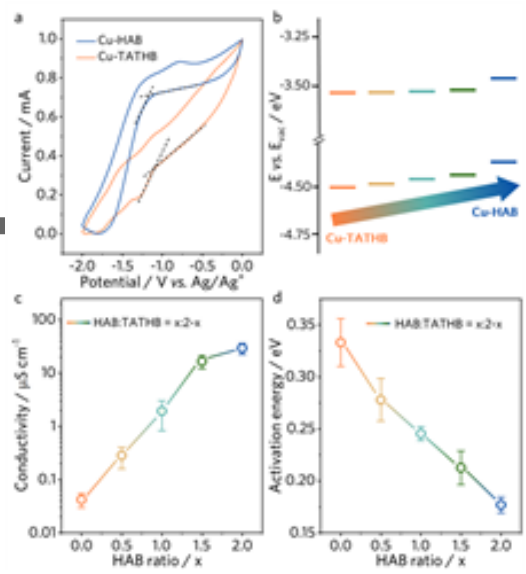

Figure 5. (a) Cyclic voltammetry of Cu-HAB and Cu-TATHB at a scan rate of 100 mV s^{-1} using an Ag/Ag^{+} reference electrode. (b) Band alignment of $Cu_3(HAB)_x(TATHB)_{2-x}$. (c) Electrical conductivity and (d) continuous changes of activation energy in $Cu_3(HAB)_x(TATHB)_{2-x}$ (x = 0, 0.5, 1, 1.5, and 2).